Progress In Electromagnetics Research C, Vol. 48, 53–60, 2014

An Improvement to Directional Equiangular Spiral Antenna with Wide CP Band, High Gain and Low Profile

Xiang Liu, Junping Geng*, Xianling Liang, Ronghong Jin, Cheng Zhang, and Kun Wang

Abstract—An improved directional equiangular spiral antenna with wide CP band and high gain is proposed, in which the impedance bandwidth is $2 \sim 12$ GHz, CP bandwidth, $4.5 \sim 7$ GHz, and gain $6 \sim 9.5$ dBi. The antenna includes 4 layers. The top layer is equiangular spiral antenna, and the bottom layer is the ground. The middle two layers are parasitic metal films with irregular rectangular holes, which are introduced to improve the performance of equiangular spiral antenna and reduce the profile. The measured results are in good agreement with the simulated ones.

1. INTRODUCTION

UWB antennas are very useful for various applications, especially in the high-speed wireless communications [1–3]. The key point of the designing of UWB antenna is how to keep its radiation performance stable in the whole frequency band, including impedance, radiation direction, gain, beam shape, etc. In some cases, it should also be in low profile and conformal. Obviously, paying attention to impedance matching only such as the design in [4], is insufficient and difficult to be conformal. The spiral antenna is a type of UWB antenna [5]. It is well known that the equiangular spiral antenna has wide bandwidth and circular polarization characteristics. But its radiation pattern is bi-directional, which may lose half of EM energy if a wave-absorber is used [6]. If the reflector is just a ground, the distance between equiangular spiral antenna and ground is fixed. Though the far-field pattern of equiangular spiral antenna is changed by the ground to be directional instead of bidirectional, the bandwidth of the antenna is restricted. In [7], a UWB spiral antenna with parabolic reflector was designed. Its bandwidth for VSWR < 1.5 was 0.94 GHz to 4.27 GHz, or $4.5 : 1$ in bandwidth ratio, but its profile was high, nearly 45 mm. A novel composite corrugated-reflector [8] was introduced to improve the directional radiation band of the printed dipole antenna and reduce its profile to 21 mm high. However, its radiation pattern was just stable from 2.5 GHz to 6.0 GHz. PBG substrate [9] and EBG structure [10] were introduced to reduce the profile of spiral antenna, but their bandwidth ratio was narrow.

In this study, two parasitic layers with irregular rectangular holes are introduced in the equiangular spiral antenna to get high gain, maintain the CP performance in a wide band and reduce its profile to 19.3 mm high. By optimizing the irregular holes, an equiangular spiral antenna with wide axial ratio band and stable pattern is obtained, and a cut-away style coaxial balun is used to feed the equiangular spiral antenna [11].

2. ANTENNA GEOMETRY

The equiangular spiral antenna with ground is marked as Ant1, in which the distance between equiangular spiral antenna and ground is fixed, and the bandwidth available with stable directional radiation is limited. When the two parasitic layers are added with some rectangular holes, the phase

Received 25 December 2013, Accepted 26 February 2014, Scheduled 7 March 2014

* Corresponding author: Junping Geng (gengjunp@sjtu.edu.cn).

The authors are with the Department of Electronic Engineering, Shanghai Jiao Tong University, 800# Dongchuan Road, Shanghai 200240, P. R. China.

of the reflected wave from the downside is different from Ant1, because part of the reflected wave is from the parasitic layers, which improves the gain and CP performance, with directional pattern and low profile in a wide bandwidth. This is marked as Ant2.

The side view of Ant2 is shown in Fig. 1(a). The top layer is equiangular spiral antenna as shown in Fig. 1(b). The two parasitic layers are shown in Fig. 1(c) and Fig. 1(d), respectively. The substrate used for the design is Taconic TLT-6 with permittivity 2.65. The two parasitic layers are set up referenced from [12]. Both parasitic layers can be divided into four rotational symmetry parts as shown in Fig. 1(c) and Fig. 1(d), which can improve the CP characteristic of the antenna. Each part includes $10 * 10$ grids. The size of the gird is $a * a$. Each grid with code is optimized by PSO in which the coding "1" represents a gird with metal and "0" a grid without metal. The distance between equiangular spiral antenna and parasitic layer 1 is set as parameter H_1. The distance between equiangular spiral antenna and ground is H_2. The interval between the two parasitic layers is a substrate, and the height depends on the substrate we bought. The interspace between parasitic layer 2 and ground is similar too. A cut-away style coaxial balun is used to feed the antenna. From the coaxial end, the outer conductor is cut away along a helix line to a tip to keep the internal reflection low. Also, a fan-shaped patch to the arm is connected to the central conductor of the balun [7, 11]. The inner and outer diameters of the coaxial are 0.436 mm and 2.2 mm, respectively, while the length of the balun is 22 mm. In our work, the simulation tool is CST, MICROWAVE STUDIO, which is based on Finite Integration in Time Domain and Finite Difference in Time Domain method. Both parasitic layers with irregular rectangular holes and parameters (a, H_1) are optimized by CST. The optimization targets include S_{11}, axial ratio and directivity of the proposed antenna. Meanwhile, an equiangular spiral antenna without the two parasitic layers serves as a contrast.

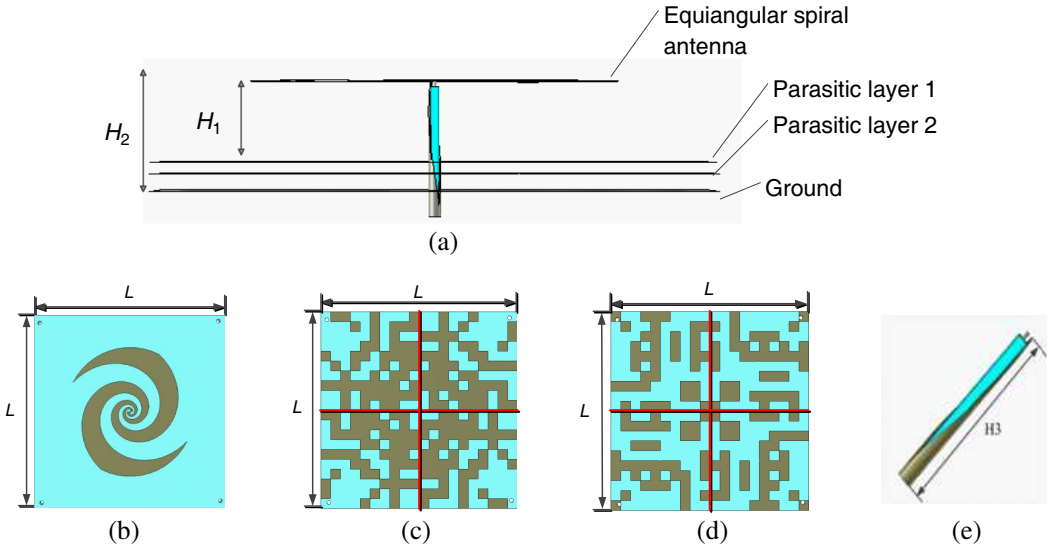

Figure 1. Ant2 structure. (a) Side view. (b) Equiangular spiral antenna. (c) Parasitic layer 1. (d) Parasitic layer 2. (e) Balun. ($H_1 = 14.3$ mm, $H_2 = 19.3$ mm, $H_3 = 22$ mm, $L = 98$ mm).

3. SIMULATED RESULTS

After optimization, the simulated S_{11} of the two antennas are shown in Fig. 2. The impedance bandwidth of the two antennas covers 2.15 GHz to 12 GHz for $S_{11} < -10$ dB. This means that, after introducing the two parasitic layers, Ant2 keeps an impedance bandwidth as good as Ant1.

The simulated far field patterns of the two antennas are shown in Fig. 3. It is very clear that the far-field patterns of Ant1 are stable from 2 GHz to 6.8 GHz, while those of Ant2 are stable from 2 GHz to 8.7 GHz. The distance between the parasitic layers and equiangular spiral antenna is shorter than that between the equiangular spiral antenna and ground. Without the parasitic layers as in Ant1, the reflected wave is just from the ground, which makes the far-field confusion at higher frequency from

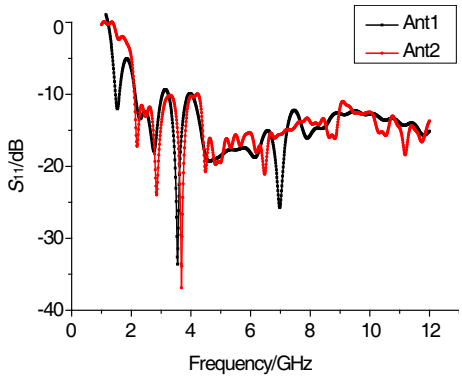

Figure 2. Simulated S_{11} of Ant1 and Ant2.

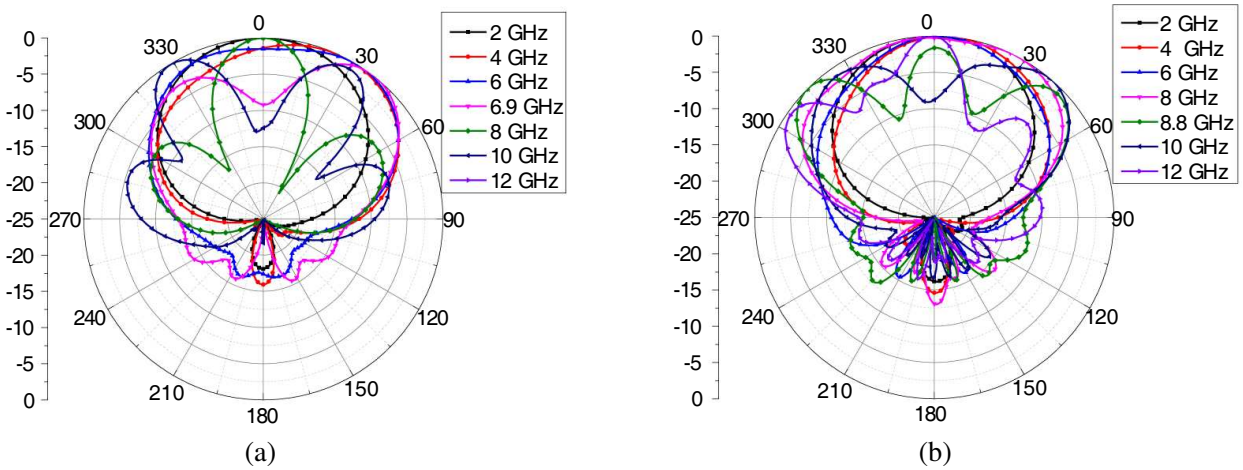

Figure 3. Simulated far field patterns of (a) Ant1 and (b) Ant2.

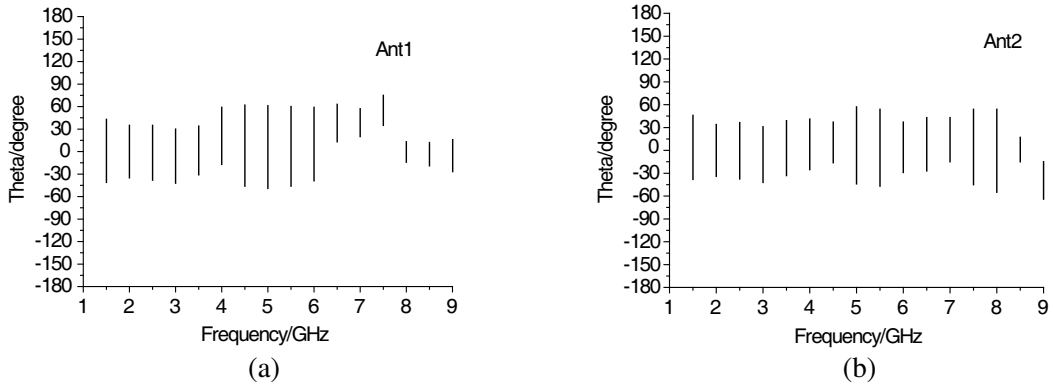

Figure 4. Simulated 3 dB beam width of (a) Ant1 and (b) Ant2.

6.8 GHz to 12 GHz. When the two parasitic layers are added as in Ant2, part of the reflected wave is from the two parasitic layers, which maintains the far-field pattern stability at high frequency from 6.9 GHz to 8.7 GHz.

Figures 4 and 5 show the 3 dB beam width and main beam directions of Ant1 and Ant2, respectively. The main beam direction of Ant2 is around Theta = 0° and varies less than that of Ant1. At low frequency 2 GHz to 4 GHz, main beam directions of both antennas are nearly the same. But at high frequency from 4 GHz to 8.6 GHz, Ant1's main beam direction is tilted away from boresight. Obviously, the main beam of Ant2 is more stable than that of Ant1, and its main beam direction is at theta = 0

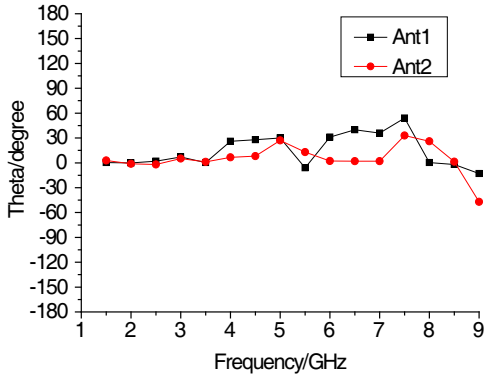

Figure 5. Simulated main beam direction of Ant1 and Ant2.

in 2 GHz $\sim$ 8.7 GHz.

Obviously, the far-field patterns of Ant2 are more stable than those of Ant1 at high frequency due to the two parasitic layers. Here we use a circularly-polarized plane wave to verify the performance of the limited ground, parasitic layers and parasitic layers with ground at high frequency (7.5 GHz). The size of the limited ground and parasitic layers are the same as those in Ant2.

Figure 6 shows that the reflected wave power flow density from the limited ground distributes around the edge. Fig. 7 and Fig. 8 show that the reflected wave power flow density from the parasitic layers and parasitic layers with limited ground are mainly rotationally and symmetrically distributed. And the density is greater especially in the central area. The transmitted wave power flow density in these cases mainly distributes around the edge that contributes to the electromagnetic diffraction. It is clear that the two parasitic layers can concentrate the reflected energy in the central area that improves the stability of patterns and gains at high frequency.

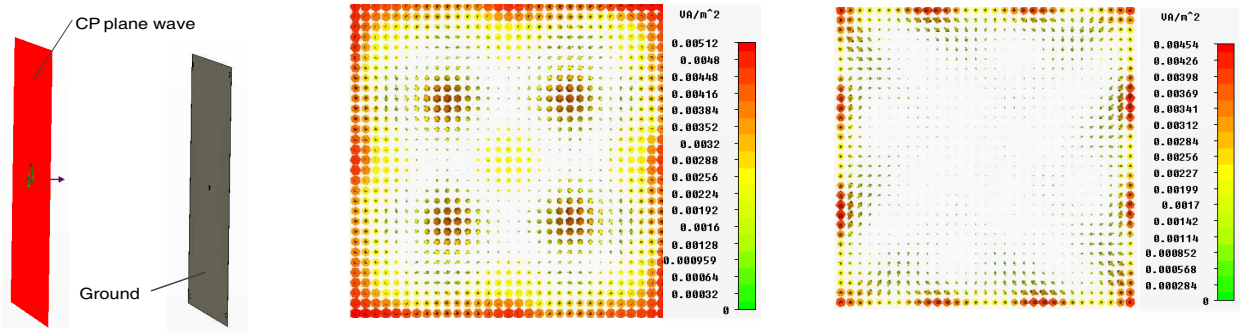

(a) (b) (c)

Figure 6. (a) Circularly polarized plane wave radiates the limited ground. (b) Simulated reflected wave power flow density at 7.5 GHz. (c) Simulated transmitted wave power flow density at 7.5 GHz.

The simulated axial ratios of Ant1 and Ant2 versus frequency are shown in Fig. 9. The simulated axial ratio of Ant1 is less than 3 dB in the band almost from 4.2 GHz to 8.9 GHz (71.2%) except in 7.2 GHz. And the simulated axial ratio of Ant2 is less than 3 dB in the band almost from 4.4 GHz to 9.5 GHz (73.4%) except the same frequency 7.2 GHz. The comparison shows that the two parasitic layers are able to broaden the spiral antenna axial ratio bandwidth in a certain extent due to the self-rotational structure of parasitic layers, and the induced surface current on the parasitic layers is almost rotated in distribution.

The simulated gains of Ant1 and Ant2 are shown in Fig. 10. From 2 GHz to 4 GHz, and the gains of the two antennas are nearly the same, but from 4.3 GHz to 7 GHz, the gain of Ant2 is higher than

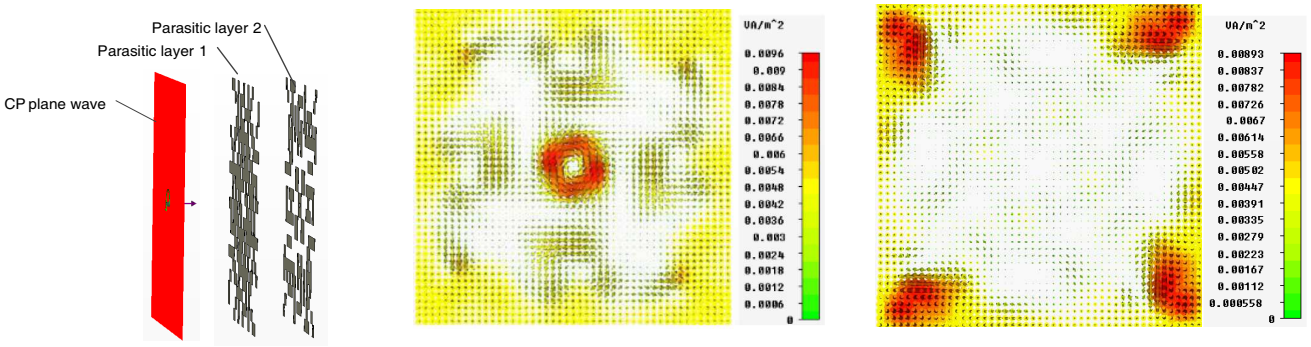

(a) (b) (c)

Figure 7. (a) Circularly polarized plane wave radiates the parasitic layers. (b) Simulated reflected wave power flow density at 7.5 GHz. (c) Simulated transmitted wave power flow density at 7.5 GHz.

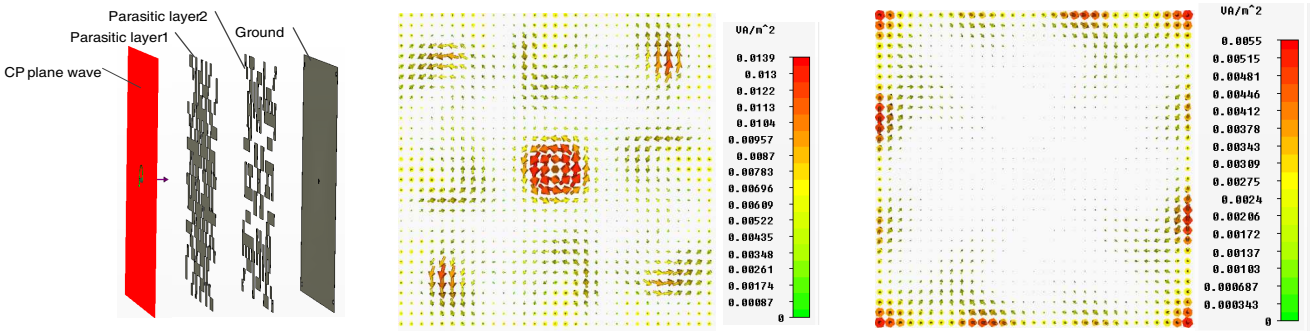

(a) (b) (c)

Figure 8. (a) Circularly polarized plane wave radiates the parasitic layers with limited ground. (b) Simulated reflected wave power flow density at 7.5 GHz. (c) Simulated transmitted wave power flow density at 7.5 GHz.

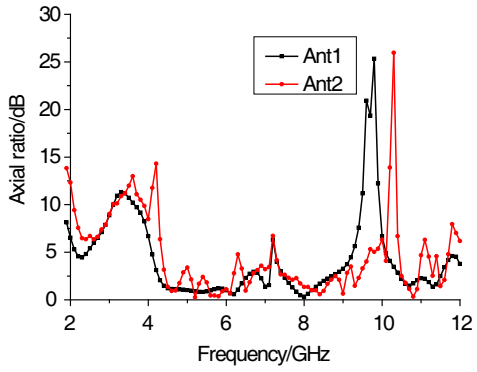

Figure 9. Simulated axial ratio of Ant1 and Ant2.

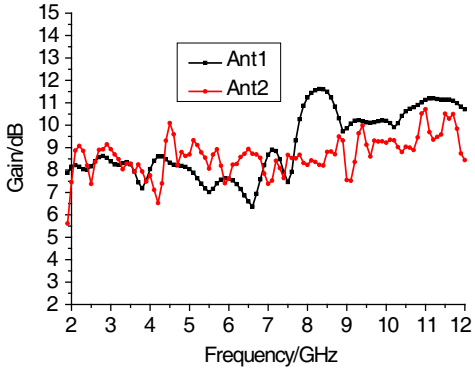

Figure 10. Simulated gain of Ant1 and Ant2.

that of Ant1. Though from 7 GHz to 12 GHz, the gain of Ant1 is higher, its far field patterns become disorderly.

From the simulated results of the two antennas and the discussion above, the two antennas cover 2.15 GHz to 12 GHz for $S_{11} < -10$ dB. The far-field patterns of Ant1 and Ant2 are stable from $2 \sim 6.8$ GHz and $2 \sim 8.7$ GHz, respectively. The AR bandwidths of the two antennas are 71.2% and 73.4%. The simulated gain of Ant2 is higher than that of Ant1 from $4.3 \sim 7$ GHz.

4. MEASUREMENT RESULTS

The fabricated Ant2 is shown in Fig. 11. The S_{11} of the fabricated antenna is shown in Fig. 12. The measured impedance matching band for $S_{11} < -10$ dB is from 2.06 Hz to 12 GHz, which is similar to the simulated result.

(a) (b) (c) (d)

Figure 11. The fabricated Ant 2. (a) Equiangular spiral antenna. (b) Parasitic layer 1. (c) Parasitic layer 2. (d) Side view.

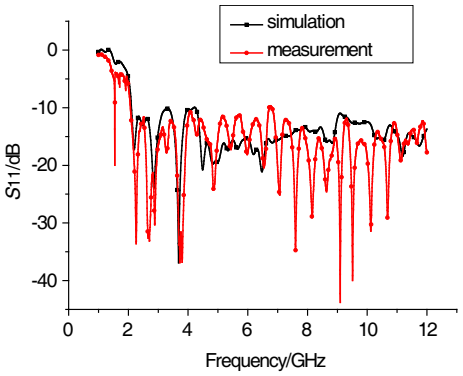

Figure 12. Simulated and measured S_{11} of the fabricated Ant2.

In Fig. 13, the simulated and measured far-field patterns of Ant2 are shown at different frequencies, and the measured results are almost the same as the simulated ones. It also shows that the far-field patterns of Ant2 are stable.

Figure 14 shows the simulated and measured axial ratios of Ant2. It is clear that the measured axial ratio of Ant2 is almost below 3.8 dB from 4.6 GHz to 8 GHz except for 7.2 GHz, which is similar to the simulated results.

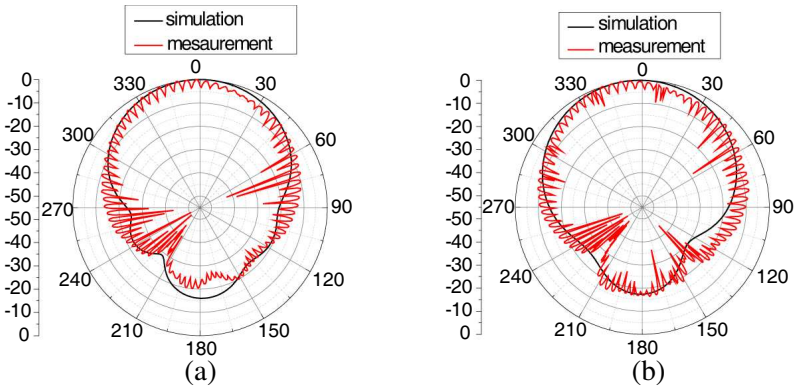

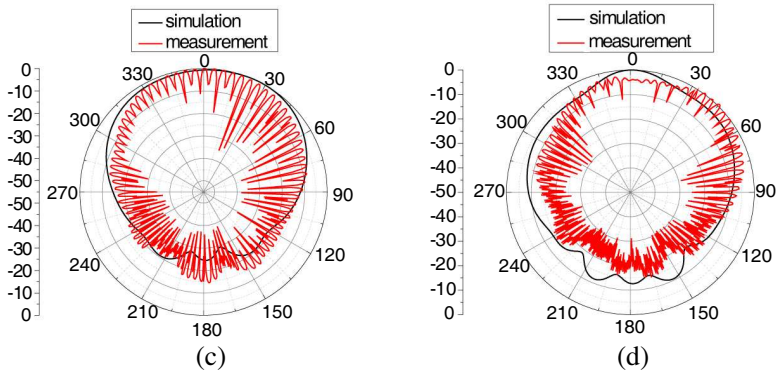

Figure 13. Simulated and measured far field pattern of the fabricated Ant2. (a) 2 GHz. (b) 3 GHz. (c) 5 GHz. (d) 7 GHz.

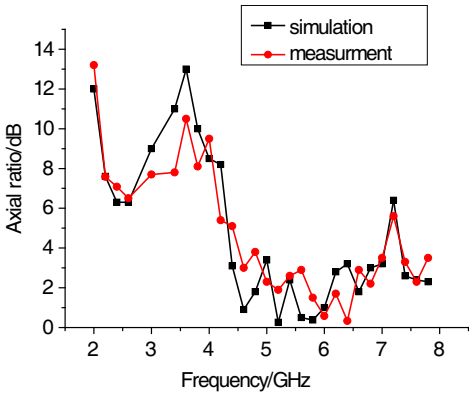

Figure 14. Simulated and measured axial ratio of the fabricated Ant2.

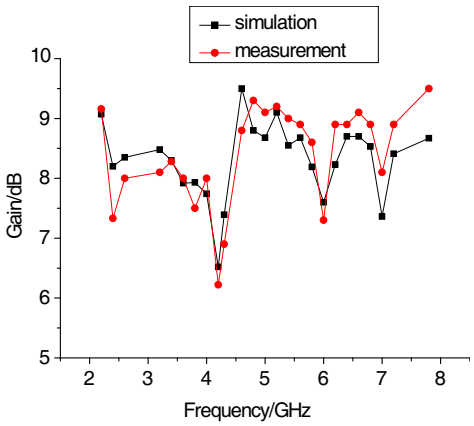

Figure 15. Simulated and measured gain of the fabricated Ant2.

In Fig. 15, the simulated and measured gains of Ant2 are shown. The trends of the simulated and measured gains are similar. The measured gain is $6.22 \sim 9.5$ dB.

5. CONCLUSION

In this paper, two parasitic layers are introduced to improve the performance of the equiangular spiral antenna with more stable far-field patterns, a broader axial ratio bandwidth and a higher gain. Its measured impedance match bandwidth is from 2.06 GHz to 12 GHz at $|S_{11}| < -10$ dB. And its far-field pattern is stable from 2 GHz to 8.7 GHz. The measured axial ratio of the proposed antenna is almost below 3.8 dB from 4.6 GHz to 8 GHz except for near 7.2 GHz, which means that the proposed antenna has CP characteristic in the limited band. The profile of the proposed antenna is very low, and the height is only about 1/8 wavelength at 2.06 GHz.

ACKNOWLEDGMENT

This work was supported by the National Natural Science Foundation of China (61201058), the Dean's fund (2013002), the Project of "SMC Excellent Young Faculty", the Research and Innovation Project of Shanghai Education Commission (12Z112030001), and the Scientific Research Foundation for Returned Overseas Chinese Scholars, State Education Ministry.

REFERENCES

1. Kushwaha, N. and R. Kumar, "An UWB fractal antenna with defected ground structure and swastika shape electromagnetic band gap," *Progress In Electromagnetics Research B*, Vol. 52, 383–403, 2013.
2. Chen, D. and C. H. Cheng, "A novel compact ultra-wideband (UWB) wide slot antenna with via holes," *Progress In Electromagnetics Research*, Vol. 94, 343–349, 2009.
3. Tilanthe, P., P. C. Sharma, and T. K. Bandopadhyay, "A compact UWB antenna with dual band rejection," *Progress In Electromagnetics Research B*, Vol. 35, 389–405, 2011.
4. Ding, M., R. Jin, and J. Geng, "Optimal design of ultra wideband antenna using a mixed model of 2-D genetic algorithm and finite-difference time-domain," *Microwave and Optical Technology Letters*, Vol. 49, No. 12, 3177–3180, 2007.
5. Liu, Q., C. L. Ruan, L. Peng, et al., "A novel compact archimedean spiral antenna with gap-loading," *Progress In Electromagnetics Research Letters*, Vol. 3, 169–177, 2008.
6. Thaysen, J., K. B. Jakobsen, and H.-R. Lenler-Eriksen, "Wideband cavity backed spiral antenna for stepped frequency ground penetrating radar," *2005 IEEE Antennas and Propagation Society International Symposium*, Vol. 1B, 418–421, 2005.
7. Lao, J., R. H. Jin, and J. P. Geng, "UWB spiral antenna with parabolic reflector," *XXIX URSI General Assembly*, Chicago, Illinois, USA, 2008.
8. Wu, Q., R. Jin, J. Geng, and D. Su, "On the performance of printed dipole antenna with novel composite corrugated-reflector for low-profile ultrawideband applications," *IEEE Transactions on Antennas and Propagation*, Vol. 58, No. 12, 3839–3846, 2010.
9. Liu, T. H., W. X. Zhang, and K. F. A. Tsang, "Low profile spiral antenna with PBG substrate," *Electronics Letters*, Vol. 36, No. 9, 779–780, 2000.
10. Li, Z., G. Wang, and Y. Cao, "A low-profile equiangular spiral antenna using a novel EBG ground plane," *7th International Symposium on Antennas, Propagation & EM Theory, ISAPE'06*, 1–3, 2006.
11. Duncan, J. W. and V. P. Minerva, "100 : 1 bandwidth balun transformer," *Proceedings of the IRE*, Vol. 48, No. 2, 156–164, 1960.
12. Wu, H., J. Geng, R. Jin, et al., "An improved comprehensive learning particle swarm optimization and its application to the semiautomatic design of antennas," *IEEE Transactions on Antennas and Propagation*, Vol. 57, No. 10, 3018–3028, 2009.